Relations between Structure, Acidity, and Activity of WO_x/TiO_2: Influence of the Initial State of the Support, Titanium Oxyhydroxide, or Titanium Oxide

Vanessa Lebarbier, Guillaume Clet, and Marwan Houalla*

Laboratoire Catalyse et Spectrochimie (UMR CNRS 6506), ENSICAEN−Université de Caen, 6 Bd. du Maréchal Juin, 14050 Caen (Cedex), France

Received: July 4, 2006; In Final Form: August 25, 2006

Two series of WO_x/TiO_2 catalysts, containing W surface densities up to 4.4 W atoms/nm^2, were prepared by pore volume impregnation of two different supports, titanium oxyhydroxide (amorphous) or titanium oxide (crystallized, 100% anatase). The influence of W surface density and the nature of the support on the surface structure, development of the acidity, and catalytic performances were examined. The texture and structure of the catalysts were investigated by Brunauer−Emmett−Teller measurements, X-ray diffraction (XRD), and Raman and infrared spectroscopy. The catalytic activity was tested for 2-propanol dehydration and *n*-hexane isomerization. For catalysts obtained by impregnation of titanium oxide, XRD and Raman results showed that W was present as a surface phase. Infrared spectra indicated an increase in the degree of polymerization of W species with increasing W surface density. CO and lutidine adsorption, followed by infrared spectroscopy, showed an increase in the strength and abundance of Brønsted acid sites (measured after lutidine desorption at 573 K) with the W surface density above a threshold of 1.3 W atoms/nm^2. The development of Brønsted acidity correlated with the evolution of the infrared bands attributed to polymerized W species. A direct relationship was observed between the concentration of Brønsted acid sites and the catalytic activity for 2-propanol dehydration. Catalytic activity, for *n*-hexane isomerization, appears to be associated with the presence of highly condensed W species. The catalysts synthesized by impregnation of titanium oxyhydroxide exhibited a comparable behavior. Hence, for a given W surface density, the W surface structure, concentration of Brønsted acid sites, and catalytic performances were similar. Thus, no significant effect of the initial form of the support (titanium oxyhydroxide versus titanium oxide; 100% anatase) was evidenced.

1. Introduction

Supported tungsten oxides catalyze a large number of industrially important reactions. For example, WO_3/Al_2O_3 catalysts are known for catalyzing the skeletal isomerization of *n*-butene to isobutene,[1,2] a precursor for the synthesis of methyl-*tert*-butyl-ether, a gasoline additive. WO_3/SiO_2 catalysts are effective for the metathesis of 1-octene and 1-heptene, which are used for the synthesis of detergents.[3−5] V-promoted WO_x/TiO_2 catalysts are industrially used for the selective catalytic reduction of NO_x by ammoniac (selective catalytic reduction process).[6−12]

In particular, the WO_x/ZrO_2 system has received a great deal of attention as catalysts for *n*-alkane isomerization since the pioneering work of Hino and Arata.[13,14] It was considered as a promising alternative to less environmentally friendly sulfated zirconia. According to these authors, catalysts prepared by impregnation of Zr-oxyhydroxide, "hydrated zirconias", are active for alkane isomerization, whereas those obtained by impregnation of crystallized zirconia were reportedly not active. Similar results were reported for WO_x/TiO_2.[15] Specifically, catalysts prepared by impregnation of amorphous titanium oxyhydroxide were active for isopentane isomerization, whereas those synthesized with titanium oxide exhibited little or no activity for the same reaction.

However, recent work by our group[16] indicated that the initial form of the support, zirconium oxyhydroxide or zirconia in tetragonal form, did not affect the development of the surface structure, acidity, and catalytic properties of WO_x/ZrO_2. Our results suggest that the poor performance attributed to catalysts obtained by impregnation of crystalline zirconia is associated with the monoclinic form of the support. It is thus of interest to extend the study to the WO_x/TiO_2 system by comparing the structure and catalytic performance of WO_x/TiO_2 obtained by impregnation of titanium oxyhydroxide (amorphous) and crystalline titanium oxide in the anatase form. Previous studies of the WO_x/TiO_2 system focused on the structure of the catalysts[17−27] or the acidity.[28−33] Few studies have attempted to establish a relation with catalytic activity.[30,32,34−36] The purpose of the present work is 3-fold: (i) to study the development of the surface structure, acidity, and catalytic performance of tungsten oxides supported on titanium oxyhydroxide or titanium oxide; (ii) to investigate possible correlations among these parameters; and (iii) to infer, by comparison of the two systems, the eventual influence of the initial form of the support on the structure, acidity, and catalytic properties of the final solids.

2. Experimental Section

2.1. Preparation of the Catalysts. Two different supports were prepared from titanium oxyhydroxide. Titanium oxyhydroxide was obtained by precipitation from titanium propylate [$Ti(OPr)_4$ 97%; Aldrich] with water while stirring (molar ratio water/propylate = 105). After 1 h of stirring, the solution was filtered; the powder was washed with water and finally dried at

* To whom correspondence should be addressed. Tel.: +33-231-56-73-51. Fax: +33-231-45-28-22. E-mail: marwan.houalla@ensicaen.fr

10.1021/jp064202e CCC: $33.50
Published on Web 10/24/2006

393 K. Titanium oxyhydroxide thus obtained was then separated into two parts. The first part noted "amorphous" and designated as ZT120 was used directly as a support. The second part was calcined in air at 773 K for 3 h to yield what will be referred to as crystallized titanium oxide (solid named ZT500).

From these two supports, two series of catalysts were prepared by pore volume impregnation with ammonium metatungstate. After impregnation, the samples were dried for 16 h at 393 K and calcined at 823 K in air for 3 h. Catalysts synthesized with the amorphous support (i.e., dried at 393 K) were designated as 120WT*x;* those obtained from the crystallized support (i.e., calcined at 773 K) were designated as 500WT*x* where *x* refers to the surface density in W atoms/nm^2. The W content was measured by inductively coupled plasma−atomic emission spectrometry.

The terms 120WT0 and 500WT0 refer respectively to the amorphous (dried at 393 K) or the crystallized (calcined at 773 K) supports, impregnated with water at pH = 5.15 and calcined at 823 K for 3 h.

2.2. Brunauer−Emmett−Teller (BET) Surface Area. Nitrogen adsorption was measured at 77 K with an automatic adsorptiometer (Micromeritics ASAP 2000). The samples were pretreated at 573 K for 2 h under a vacuum. The surface areas were determined from adsorption values for five relative pressures (P/P_0) ranging from 0.05 to 0.2 using the BET method. The pore volumes were determined from the total amount of N_2 adsorbed between $P/P_0 = 0.05$ and $P/P_0 = 0.98$.

2.3. X-ray Diffraction. X-ray powder diffraction spectra were recorded using a Philips X'pert diffractometer with a copper anode ($K\alpha_1 = 0.154\ 05$ nm) and a scanning rate of $0.025°\ s^{-1}$. Data were acquired between $2\theta = 20°$ and 80°.

2.4. Raman Spectroscopy. Raman studies were performed on samples in powder form exposed to ambient conditions. The Raman spectrometer consisted of a confocal microscope Labram 300 (Jobin Yvon), equipped with a He−Ne laser (frequency 632.8 nm) and a charge-coupled device (CCD) detector. The power on the sample was generally about 8 mW. The spectra were recorded over 3 s in the 30−1500 cm^{-1} region.

2.5. Infrared Spectroscopy. *2.5.1. Study of the Catalysts by 2,6-Dimethylpyridine (Lutidine) Adsorption.* Infrared spectra were recorded with a Nicolet Avatar Fourier transform infrared (FT-IR) spectrometer equipped with a deuterated triglycine sulfate (DTGS) detector (resolution: 4 cm^{-1}, 128 scans). The samples, pressed into pellets (ca. 20 mg for a 2 cm^2 pellet), were pretreated at 723 K for 2 h in an air flow, then at 423 K in vacuum for 1 h and then cooled to 293 K. 2,6-dimethylpyridine (lutidine) was introduced at 293 K ($P_{equilibrium} = 133$ Pa), following pretreatment. The spectra were then recorded following desorption from 323 to 573 K. The number of Brønsted acid sites titrated by 2,6-dimethylpyridine was calculated using an integrated molar absorption coefficient value of $\epsilon = 6.8$ cm μmol^{-1} [37] for the sum of the ($\nu_{8a} + \nu_{8b}$) vibrations of protonated lutidine ($DMPH^+$) at ca. 1644 and 1628 cm^{-1}.

2.5.2. Study of the Catalysts by Adsorption of CO at 77 K. IR spectra were recorded with a Nicolet Magna 750 spectrometer, equipped with a mercury cadmium telluride (MCT) detector. As for lutidine adsorption, samples were pressed into pellets and pretreated at 723 K for 2 h in an air flow, then at 423 K in vacuum for 1 h. Following activation, the cell temperature was lowered to 77 K. Small doses of CO were then added up to an equilibrium pressure of 133 Pa.

2.6. Catalytic Activity. Two test reactions were used: 2-propanol dehydration and *n*-hexane isomerization. Both tests were carried out in a fixed-bed flow reactor, with the catalyst mixed with an inert solid.

TABLE 1: Composition and Texture of the Solids

sample	atoms of W/nm^2	% W	surface area ($m^2\ g^{-1}$)	pore volume ($cm^3\ g^{-1}$)
ZT120[a]	0	0	220	0.29
120WT0[b]	0	0	72	0.17
120WT0.9	0.9	2.6	91	0.19
120WT1.3	1.3	3.9	99	0.20
120WT1.6	1.6	5.5	113	0.22
120WT2.4	2.4	7.5	119	0.22
120WT3.3	3.3	12	126	0.22
120WT4.2	4.2	17.2	133	0.21
ZT500[c]	0	0	125	0.26
500WT0[b]	0	0	79	0.21
500WT0.8	0.8	2.5	102	0.24
500WT1.3	1.3	4.2	103	0.23
500WT1.5	1.5	5.1	114	0.23
500WT2.4	2.4	7.9	106	0.22
500WT3.6	3.6	11.3	102	0.21
500WT4.4	4.4	13.1	98	0.19

[a] ZT120: dried at 393 K. [b] 120WT0 and 500WT0 correspond respectively to the solids ZT120 and ZT500, after impregnation with water (pH = 5.15) and further calcination at 823 K for 3 h. [c] ZT500: TiO_2 obtained from titanium oxyhydroxide ZT120 and calcination at 773 K.

For 2-propanol dehydration, 20 mg of the catalyst mixed with 80 mg of α-Al_2O_3 were pretreated at 723 K in N_2 for 2 h (60 mL min^{-1}). The reaction was performed at atmospheric pressure with N_2 as the carrier gas ($P_{2-propanol} = 1.09$ kPa) from 373 to 413 K for various weight hourly space velocities (WHSV; 8.7 mmol h^{-1} g^{-1}). Reactants and products were analyzed with an online gas chromatograph (HP 5890 Series II) equipped with a capillary column (CP WAX 52 CB) and a flame ionization detector. The propene formation rates presented here were calculated from the mean conversion during the first hour of reaction. Similar results were obtained when the catalyst was pretreated in an air flow instead of N_2.

For *n*-hexane isomerization, 500 mg of the catalyst, mixed with 1.5 g of silicium carbide, were pretreated at 673 K for 2 h in an air flow. The reactor was flushed with a helium flow while lowering the temperature to 523 K. The catalyst was then pretreated with (1/3.5) H_2/He mixture (488 mL min^{-1}) for 1 h. *n*-hexane (300 kPa) was then vaporized in the mixture H_2−He (total pressure, 5×10^3 kPa; $P(H_2) = 10^3$ kPa) and the mixture reacted in the catalytic bed at 523 K.

3. Results

3.1. Composition and Texture of the Solids. The surface area and pore volume of the solids are shown in Table 1. For both series, higher surface areas were observed for W-containing catalysts as compared to the support.

3.2. X-ray Diffraction. Figure 1 shows the diffraction patterns of representative solids from both series between $2\theta = 20°$ and 40°. Two lines at 25.4° and 38°, characteristic of anatase, are observed. Diffraction lines characteristic of rutile ($2\theta = 27.5°$) or tungsten oxide ($2\theta = 23.1$, 23.6, 24.4°) were not detected. For both series, X-ray diffraction (XRD) patterns of the 120WT0 and 500WT0 supports show peaks narrower than those observed for W-containing solids, indicating a larger mean size of the anatase crystallites. This is consistent with lower surface areas measured for the supports.

3.3. Raman Spectroscopy. Figure 2 shows the Raman spectra, in the 550−1050 cm^{-1} region, recorded under ambient conditions, for various solids from the 120WT and 500WT series. The spectra show bands of the anatase phase at 640, 517,

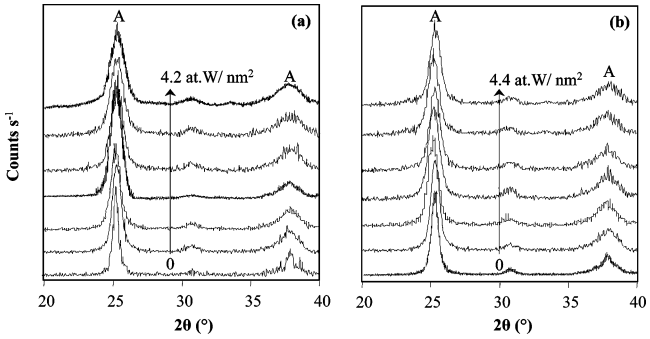

Figure 1. XRD patterns for the solids of the 120WT (a) and 500WT (b) series.

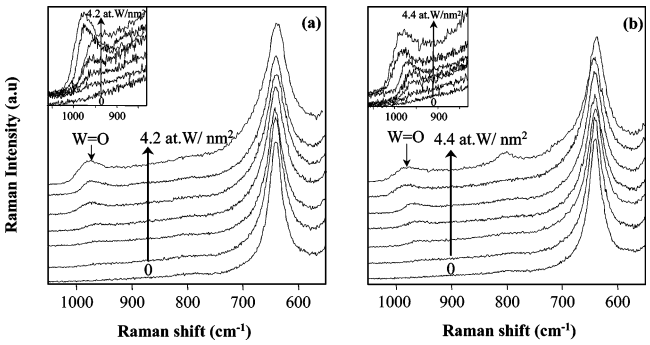

Figure 2. Raman spectra of the 120WT (a) and 500WT (b) series, normalized to the anatase band at 640 cm^{-1}. Insets: Enlargement of the 850−1050 cm^{-1} region.

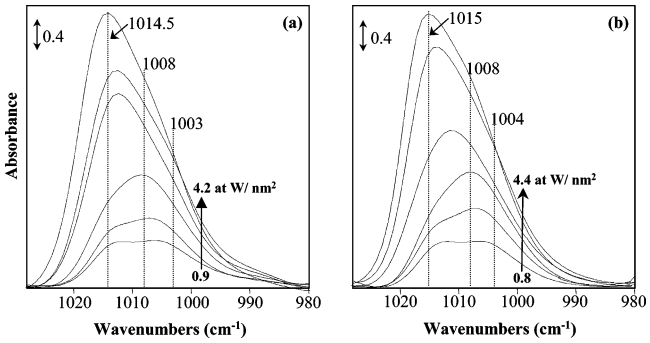

Figure 3. Infrared spectra for catalysts activated in the air at 723 K for 120WT (a) and 500WT (b) series after subtraction of the spectrum of 120WT0 or 500WT0, respectively. The spectra were normalized to 100 mg of the catalyst.

and 399 cm^{-1}.[21,28] A band observed in the ν(W═O) vibration region between 1020 and 920 cm^{-1} is attributed to W surface species.[38] The intensity of this band increased with increasing W surface density and shifted to higher wavenumbers (see the inset in Figure 2). Generally, in agreement with XRD results, bands characteristic of rutile (447 cm^{-1}) or tungsten oxide WO_3 (807 and 713 cm^{-1}) were not observed. Only for the 500W4.4 solid were indications (a small peak at ca. 805 cm^{-1} and an apparent shoulder at ca. 710 cm^{-1}) for the formation of a minor amount of WO_3 found.

3.4. Infrared Spectroscopy. *3.4.1. Structure.* FT-IR spectra of the solids after activation in air at 723 K (Figure 3) show a band in the 980−1028 cm^{-1} region attributed to ν(W═O) vibrations of surface mono-oxo tungstate species.[29,36,39] For both series, Figure 3 shows, in the 1028−980 cm^{-1} region, an increase of the band area with W surface density. For the same W surface density, spectra for both series were similar. For W surface density ≤ 1.3 at W/nm^2, the spectra showed two maxima at 1003−1004 cm^{-1} and 1012−1013 cm^{-1}. For higher values, the spectra showed only one asymmetric band with the maximum shifting with W surface density from 1008 to 1015 cm^{-1}.

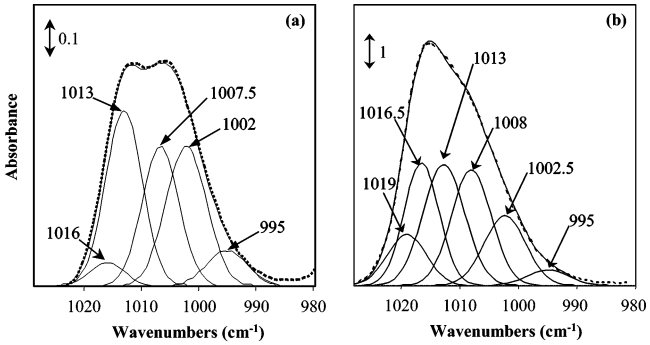

Figure 4. Curve-fitting of the infrared spectra for solids 500WT0.8 (a) and 500WT4.4 (b) after activation in the air at 723 K. Spectra were curve-fitted after normalization to 100 mg of the solid and subtraction of the spectrum of the support. Dotted line: experimental spectra. Full line: reconstituted spectra.

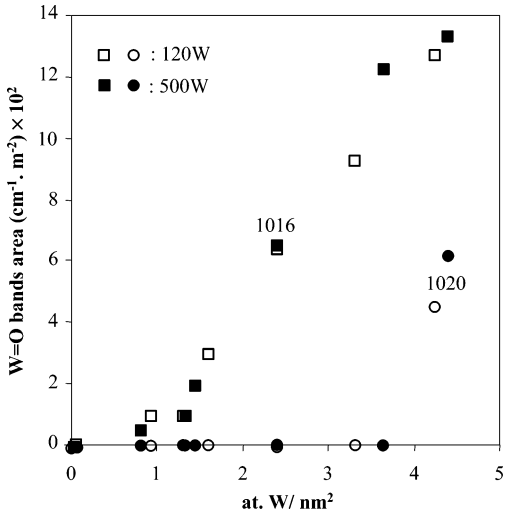

Figure 5. Evolution, with W surface density, of the band areas of the infrared ν(W═O) vibrations at 1016 (squares) and 1020 cm^{-1} (circles). Open symbols: 120WT series. Full symbols: 500WT series.

Spectra were curve-fitted in the 1028−980 cm^{-1} region. To account for the different peaks and shoulders on all of the solids, the spectra were curve-fitted with five to six bands. Reconstituted spectra were in agreement with those obtained from experiments. Two examples for catalysts 500WT0.8 and 500WT4.4 are given in Figure 4. Five bands, with Gaussian profile, located at 1016.5, 1012.5, 1008, 1002.5, and 995 ± 0.5 cm^{-1} were used for the decomposition. The full width at half maximum (fwhm) was typically 8 ± 0.5 cm^{-1}. For catalysts with W surface density > 3.6 at W/nm^2, an additional band at 1019.5 ± 0.5 cm^{-1} was detected.

The evolution of the area of the bands at 1016 and 1020 cm^{-1} with W surface density is plotted in Figure 5 for catalysts of both series. The results show that the band at 1016 cm^{-1} is detected for W surface densities ≥ 1.3 at W/nm^2. Its area increases with further increases in W surface density. The band at 1020 cm^{-1} was only observed for the highest W surface density examined (4.2−4.4 W atoms/nm^2)

3.4.2. Acidity. The development of the acidity was monitored by adsorption of two different probe molecules: 2,6-dimethylpyridine and CO.

3.4.2.1. Adsorption of 2,6-Dimethylpyridine (Lutidine). Figure 6 shows infrared spectra of the solids of both series between

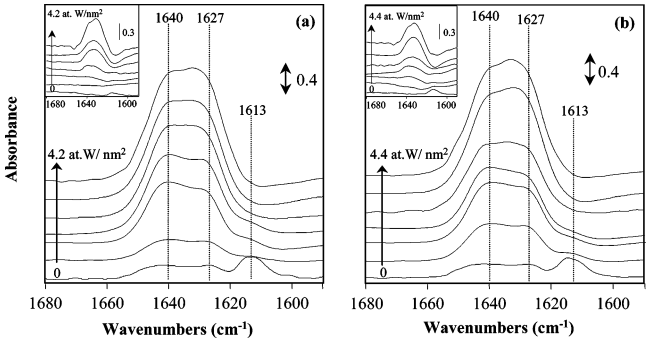

Figure 6. Infrared spectra for solids of the 120WT (a) and 500WT (b) series following the desorption of lutidine at 423 K. Insets: Spectra following the desorption of lutidine at 573 K. The spectra are normalized to 100 mg of the solid.

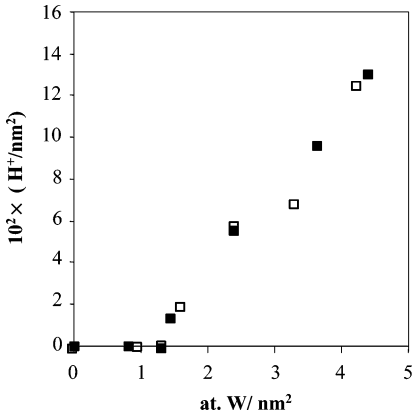

Figure 7. Evolution of the abundance of Brønsted acid sites with W surface density, measured after the desorption of lutidine at 573 K for the 120WT (□) series and 500WT (■) series.

1680 and 1590 cm^{-1} following the adsorption of lutidine and desorption at 423 K and at 573 K (insets in Figure 6). At 423 K, a doublet is observed between 1660 and 1620 cm^{-1}, characteristic of protonated lutidine on Brønsted acid sites.[40,41] Two bands appear at 1613 and 1580 cm^{-1} (not shown) attributed to coordinated lutidine and characteristic of Lewis acid sites.[40,42,43]

The concentration of Brønsted acid sites present following the desorption of lutidine at 573 K is plotted in Figure 7 as a function of W surface density. The results clearly show that Brønsted acid sites are only detected above a threshold of 1.3 atoms of W/nm^2. Their concentration increases steadily with W surface density. Figure 7 also shows that the abundance of these acid sites is essentially a function of W surface density.

3.4.2.2. CO Adsorption at Low Temperatures. A. ν(CO) Region. Figure 8 shows the infrared spectra for the solids of both series between 2110 and 2230 cm^{-1} following the admission of 133 Pa of CO at 77 K. The supports 120WT0 and 500WT0 show four main bands at 2179, 2165, 2156, and 2140 cm^{-1}. The bands and shoulders above 2156 cm^{-1} were attributed to Lewis acid sites.[44−48] The band at 2156 cm^{-1} and the shoulder at 2151 cm^{-1} were attributed to Brønsted acid sites.[44,49−51] The band at 2140 cm^{-1} is assigned to physisorbed CO.

W addition brings about significant modifications in the infrared spectra. The bands at 2179 and 2156 cm^{-1} appear to shift, respectively, to 2195 and 2167 cm^{-1} with increasing W surface density. At a low W surface density (from 0.8 to 1.6 atoms of W/nm^2), two shoulders can also be seen at 2165−2167 cm^{-1} and 2151−2153 cm^{-1}, whereas only one is observed at 2155−2159 cm^{-1} for higher loadings. For a given W surface density, the spectra of the catalysts of both series were comparable.

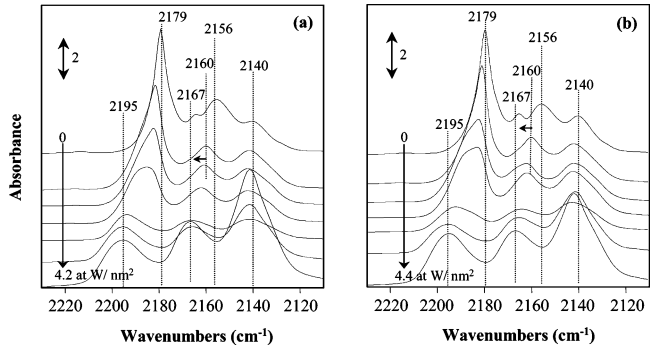

Figure 8. Infrared spectra for solids of 120WT (a) and 500WT (b) series recorded after the introduction of 133 Pa CO at equilibrium. The spectra were normalized to 100 mg of the solid. W surface density increases downward.

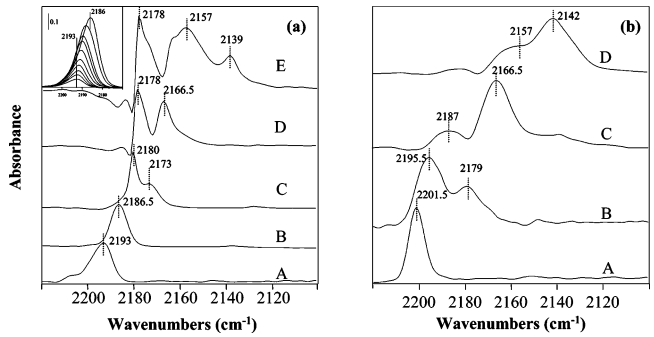

Figure 9. Infrared spectra recorded after increasing the addition of small doses of CO for 500WT0 (a) and 500WT3.6 (b) samples. Each spectrum was obtained by subtraction from the observed spectrum that recorded for the previous dose of CO. The total amount of CO added increases from A to E.

3.4.2.2.B. Curve-Fitting: ν(CO) Region. Figure 9a (inset) illustrates an example of the evolution of the CO bands, in a given region, upon the incremental addition of CO. The positions of the CO vibrations attributed to different acid sites are obtained by subtracting from the observed spectrum that recorded for the previous CO dose. The results for 500WT0 (a) and 500WT3.6 (b) are shown in Figure 9. For the 500WT0 solid, bands are detected at 2193 cm^{-1} (spectrum A); 2186.5 cm^{-1} (spectrum B); 2180 and 2173 cm^{-1} (spectrum C); 2178 and 2166.5 cm^{-1} (spectrum D); and 2178, 2157, and 2139 cm^{-1} (spectrum E). For the 500WT3.6 sample, bands are observed at 2201.5 cm^{-1} (spectrum A), 2195.5 and 2179 cm^{-1} (spectrum B), 2187 and 2166.5 cm^{-1} (spectrum C), and 2157 and 2142 cm^{-1} (spectrum D). For both samples, the development of the bands with CO addition indicates a selective titration of the most acidic site by the probe molecule.

The spectra obtained following CO addition were curve-fitted for each solid using the positions of the observed peaks (and shoulders) and those of the bands shown above (Figure 9a,b). Figure 10 shows two examples of curve-fitting (for spectra recorded after the admission of 133 Pa CO at equilibrium) for 500WT0 (a) and 500WT3.6 (b) solids.

The results for the 500WT0 solid show bands at 2194, 2186, 2179.5, 2172, and 2165.5 (fwhm = 7.5 ± 1 cm^{-1}) attributed to Lewis acid sites; bands at 2157 and 2151 (fwhm = 11± 1 cm^{-1}) ascribed to Brønsted acid sites; and a band at 2140 cm^{-1} due to physisorbed CO. For the 500WT3.6 solid, bands attributed to Lewis acid sites appeared at 2202, 2195, 2187, and 2178 cm^{-1} (fwhm = 9 ± 1 cm^{-1}); those ascribed to Brønsted acid sites were detected at 2167.5 and 2158 cm^{-1} (fwhm = 11 ± 1 cm^{-1}), and the band characteristic of physisorbed CO was located at 2141 cm^{-1}. Curve-fittings of the spectra for all of

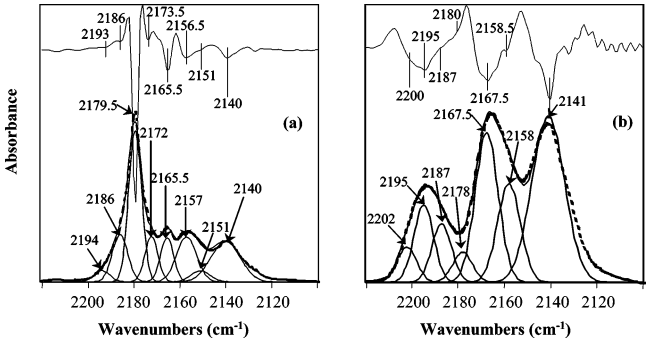

Figure 10. Curve-fitting of the IR spectra of 500WT0.8 (a) and 500WT3.6 (b) (133 Pa CO). Dotted lines: experimental spectrum. Full lines: reconstituted spectrum. The curves on the upper part of the figures are the second derivatives of the experimental spectra.

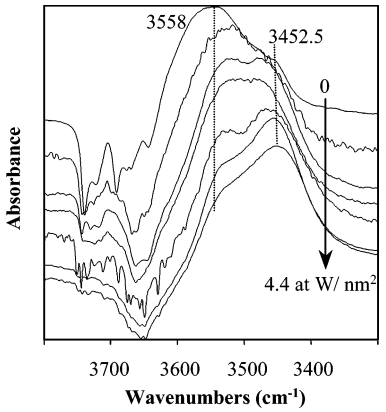

Figure 11. Infrared spectra for solids of the 500WT series after the introduction of 133 Pa CO and subtraction of the spectrum recorded before CO introduction. W surface density increases downward.

the samples required the use of six bands characteristic of Lewis and Brønsted acid sites. These bands shift with increasing W surface density, respectively from 2194, 2186, 2179.5, and 2172 cm^{-1} to 2202, 2195, 2188, and 2179 cm^{-1} and from 2157 and 2151 cm^{-1} to 2169 and 2159 cm^{-1}. An additional band located at 2166−2168 cm^{-1} (fwhm = 11 ± 1 cm^{-1}) was detected for solids with W surface densities ≤ 1.6 atoms of W/nm^2.

3.4.2.2.C. ν(OH) Region. Figure 11 shows the infrared spectra for the solids of the 500WT series, between 3300 and 3800 cm^{-1}, following the introduction of 133 Pa CO at equilibrium (after subtraction of the spectra of the same solid recorded before the introduction of CO). It can be seen that CO addition leads to a shift in the position of the hydroxyls vibrations from 3600−3800 cm^{-1} to 3400−3600 cm^{-1}. For all of the solids, the spectra recorded after the introduction of 133 Pa CO reveal two bands at 3440−3480 cm^{-1} and 3530−3560 cm^{-1}. The position of the maximum of the envelope shifts with increasing W surface density from 3558 cm^{-1} (500WT0) to 3452.5 cm^{-1} (500WT4.4). Similar results were obtained from the spectra of solids of the 120WT series.

3.4.2.2.D. Curve-Fitting: ν(OH) Region. The spectra recorded after the introduction of small doses of CO were also curve-fitted in the hydroxyl region between 3300 and 3800 cm^{-1}. Figure 12 shows two examples of curve-fitting [500WT0 (a) and 500WT3.6 (b)] for spectra recorded after the introduction of 133 Pa CO at equilibrium. Two bands at ca. 3460 and 3540 cm^{-1} are detected.

Curve-fitting results for the 500WT series are reported in Table 2. Similar results were obtained for solids of the 120WT series.

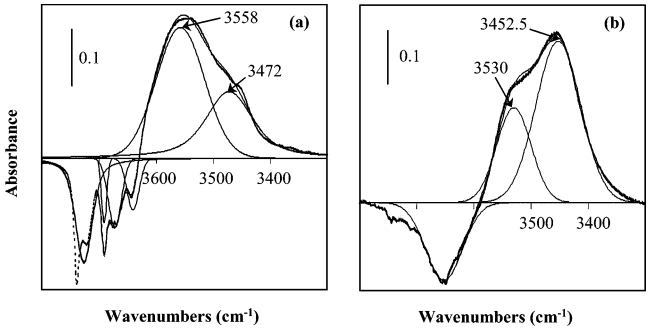

Figure 12. Curve-fitting of the infrared spectra of 500WT0 (a) and 500WT3.6 (b) following the introduction of 133 Pa CO at equilibrium and subtraction with the spectrum of the same solid recorded before the introduction of CO.

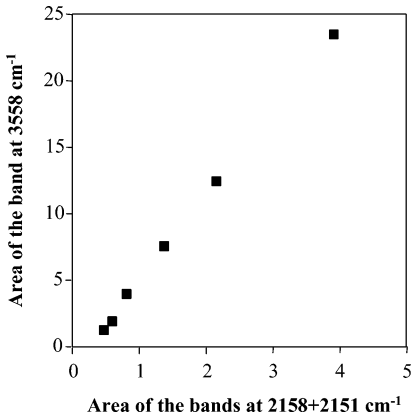

Figure 13. Infrared spectroscopy results after CO adsorption for 500WT0. Plot of the area of the ν(OH) band at 3558 cm^{-1} vs that of the ν(CO) bands at 2158 and 2151 cm^{-1}.

TABLE 2: Positions and fwhm's of the Bands Determined after Curve-Fitting of the Spectra between 3600 and 3300 cm^{-1}, Recorded Following Admission of 133 Pa CO at Equilibrium

	3440−3480 cm^{-1}		3530−3560 cm^{-1}	
solid	position (cm^{-1})	fwhm (cm^{-1})	position (cm^{-1})	fwhm (cm^{-1})
500WT0	3472	89	3558	100
500WT0.8	3456	89	3538	100
500WT1.3	3455.5	83	3532.5	84
500WT1.5	3455	91	3530	100
500WT2.4	3462	100	3539	59
500WT3.6	3452.5	92	3530	71
500WT4.4	3446	95	3523	73

3.4.2.2.E. Relations between ν(OH) and ν(CO) Vibrations. Curve-fitting of the spectra after the addition of CO allowed the monitoring of the area of the bands between 3400 and 3600 cm^{-1} [ν(OH)] and that of the bands between 2151 and 2169 cm^{-1}. The results are shown in Figure 13 for the 500WT0 support. A linear relationship is observed between the total area of the bands at 2158 and 2151 cm^{-1} and the area of the band at 3558 cm^{-1}. Similar behavior was observed for catalysts with W surface density ≤ 1.6 atoms of W/nm^2. The implications of these relationships will be discussed later in this article.

For the catalysts with W surface density > 1.6 atoms of W/nm^2, linear relationships were observed between bands at 2169−2165 cm^{-1} and 3446−3462 cm^{-1} and between bands at 2159−2155 cm^{-1} and 3523−3539 cm^{-1}, indicating the presence of Brønsted acid sites of different strengths. An example is shown in Figure 14 for the 500WT3.6 catalyst. Similar relations were observed for the 120WT series.

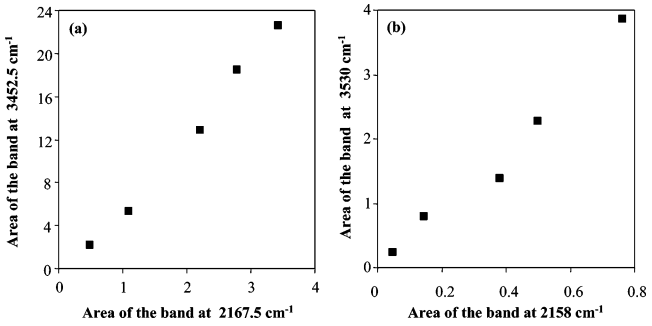

Figure 14. FT-IR spectroscopy results after CO adsorption for the 500WT3.6 catalyst: Area of the ν(OH) bands in the 3400−3600 cm^{-1} region vs the area of the ν(CO) bands in the 2158−2168 cm^{-1} region.

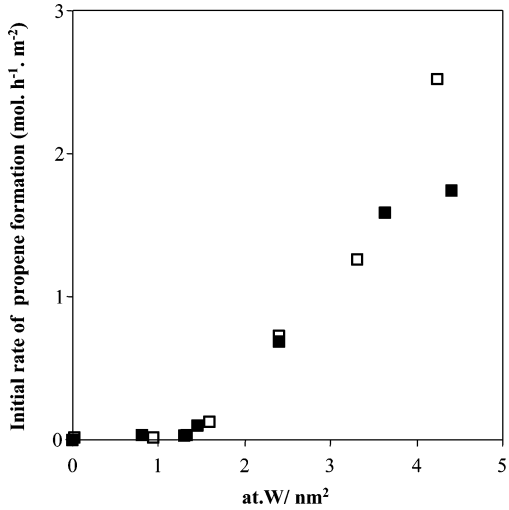

Figure 15. Initial rate of propene formation vs W surface density at $T = 403$ K and $D = 60$ mL min^{-1} for the 120WT (□) series and 500WT (■) series.

3.5. Catalytic Activity. *3.5.1. 2-Propanol Dehydration.* The activity of both series of catalysts was tested in the reaction of 2-propanol dehydration. Under the conditions adopted for the present study ($T = 373-413$ K; WHSV = 8.7 mmol h^{-1} g^{-1}), both supports 120WT0 and 500WT0 were inactive. With active catalysts, only dehydration (propene) and condensation (diisopropyl ether) products were formed. For the catalysts of both series, 120WT and 500WT, the selectivity for propene was high (between 85 and 88%). The propene formation rate is plotted in Figure 15 as a function of W surface density. For both series, no significant activity was observed below 1.3 W atoms/nm^2. Above this threshold, the activity increased with W loading. For a given W surface density, catalysts of both series showed comparable activity.

3.5.2. n-Hexane Isomerization. With active catalysts, four products only were obtained: 2-methylpentane, 3-methylpentane, 2,3-dimethylbutane, and 2,2-dimethylbutane. Their selectivities were 49%, 36%, 13%, and 2% respectively. Figure 16 shows the evolution of the initial rate of *n*-hexane isomerization versus W surface density. In this case, only the solids with a high W surface density (≥3.3 atoms of W/nm^2) were active.

4. Discussion

In a previous study, it was shown that the structure, acidity, and catalytic performance of WO_x/ZrO_2 catalysts were not significantly affected by the form of the support (amorphous or predominantly tetragonal zirconia) prior to impregnation.[16] The objective of the present work was to extend the study to the related WO_x/TiO_2 system. The latter catalysts can also be

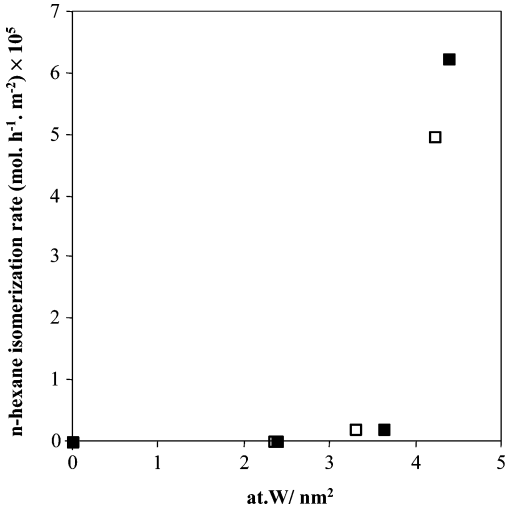

Figure 16. Initial rate of isomerization of *n*-hexane at 523 K and $P(H_2) = 10^3$ kPa for the 120WT (□) series and 500WT (■) series.

synthesized from two types of supports: amorphous titanium oxyhydroxide and crystalline titanium oxide in anatase or rutile form. In the following discussion, we will first analyze for a given series of WO_x/TiO_2 catalysts the relationship between surface structure and catalytic activity and then infer, by comparing the results of the two series, any eventual effect of the initial state of the support (amorphous titanium oxyhydroxide or crystalline titania in an anatase form).

4.1. Composition and Texture of the Support. XRD and Raman results indicate that, for both series, only titania in the anatase form was detected. Analysis of the results of Table 1 also show that, consistent with earlier studies,[29,33] W addition inhibits the sintering of the anatase phase.

4.2. Structure of W Surface Species. For the 500WT series, XRD and Raman spectroscopy results show no evidence of WO_3 formation (Figures 1 and 2). Raman and infrared results (Figures 2 and 3) indicate the presence of the bands in the 920−1030 cm^{-1} region characteristic of ν(W═O) vibration and attributed to surface mono-oxo tungstate species.[29,36,38,39] The area of these bands increases steadily with increasing W surface density, indicating a progressive buildup of W surface species. Note that, for a given W surface density, similar Raman and infrared spectra were observed for both 120WT and 500WT series (Figures 2 and 3).

For catalysts of the 500WT series, the decomposition of the envelope in the 980 and 1028 cm^{-1} regions of the infrared spectra (Figure 4a) characteristic of surface mono-oxo tungstate species[29,36,39] indicates the presence of five bands located at ca. 1016, 1012, 1008, 1002, and 995 cm^{-1}. For the catalyst with the highest W surface density (4.4 atoms of W/nm^2), an additional band at ca. 1020 cm^{-1} was detected (Figure 4b). High wavenumber bands at similar positions (1017, 1012, and 1004 cm^{-1}) were observed for catalysts obtained by the impregnation of titania (58% anatase).[32] Infrared and Raman bands at comparable positions (1021, 1017, and 1010 cm^{-1} by infrared and 978 and 1006−1016 cm^{-1} by in situ Raman) were also reported for catalysts synthesized by impregnation of titanium oxyhydroxide.[24] The shift to a higher wavenumber of the Raman band position at 1006−1016 cm^{-1} with W surface density was attributed by Eibl et al.[24] to an increased degree of condensation of W species. A similar interpretation had been proposed for the MoO_x/ZrO_2 solids.[52] This hypothesis is also consistent with the shifts observed for aqueous W species[53] with different degrees of condensation. One may thus speculate that

the multiplicity of the bands observed in the present study is indicative of various extents of polymerization of the W species.

For the 120WT series obtained by impregnation of titanium oxyhydroxide, a qualitative comparison of the infrared spectra with those obtained for the 500WT series (Figures 3 and 5) clearly illustrates the close similarity of the structure of the two systems. This is confirmed by the analysis of the envelope characteristic of the ν(W═O) vibration, which shows for a given W surface density the same bands with comparable intensities. These results are consistent with those reported for the WO_x/ZrO_2 system.[16] They indicate that the structure W surface species is not significantly affected by the initial form of the support.

4.3. Acidity. The development of the acidity was monitored by the adsorption of probe molecules lutidine and CO followed by infrared spectroscopy. The results show significant changes in Brønsted and Lewis acidity with W surface density.

4.3.1. Lewis Acidity. An infrared study of the adsorption of lutidine followed by desorption at 423 K (Figure 6), shows that the area of bands characteristics of Lewis acid sites at 1580 and 1613 cm^{-1}, attributed to Ti^{4+}, decreases with increasing W surface density. This can be ascribed to a progressive coverage of Ti^{4+} sites by W surface species.

An analysis of infrared spectra following low-temperature CO adsorption (Figure 8) shows a shift in the position of the band characteristic of Lewis acid sites from 2179 to 2195 cm^{-1}, with increasing W surface density. This indicates, as reported earlier,[29,34,36] the formation of stronger Lewis acid sites on W addition.

4.3.2. Brønsted Acidity. 4.3.2.1 Evolution of the Abundance of Brønsted Acid Sites with W Addition. The abundance of Brønsted acid sites following adsorption at ambient temperature and desorption at 573 K of lutidine has been quantified for solids of both the 500WT and 120WT series. The results reported in Figure 7 show for both systems the presence of a threshold at 1.3 atoms of W/nm^2 for the development of Brønsted acidity. This is in accord with the results reported for catalysts obtained by the impregnation of titania (58% anatase).[32] Figure 7 also shows that, for a given W surface density, similar concentrations of Brønsted acid sites are measured. Thus, as noted for the structure of W surface species, the initial form of the support (oxyhydroxide or titania in an anatase form) appears to have little or no effect on the abundance of Brønsted acid sites in the WO_x/TiO_2 catalysts. This is in accord with our previous results concerning WO_x/ZrO_2 catalysts.[16]

The concentration of Brønsted acid sites measured for both series was compared to those reported in the literature. For the supports 500WT0 and 120WT0, the concentration of Brønsted acid sites, measured after lutidine desorption at 423 K, was respectively 0.11 H^+/nm^2 and 0.14 H^+/nm^2. This is in accord with the results obtained by Lahousse et al. (ca. 0.15 H^+/nm^2) for a titania calcined at 773 K.[43] For 500WT3.6 and 120WT3.3 catalysts, the abundance of these acid sites measured after lutidine desorption at 573 K was respectively 0.1 H^+/nm^2 and 0.07 H^+/nm^2. These results are similar to those reported by our group (0.06 H^+/nm^2) for a catalyst containing 3.4 atoms of W/nm^2 [32] prepared by impregnation of titania and measured under the present conditions.

4.3.2.2. Evolution of the Strength of Brønsted Acid Sites with W Surface Density. For catalysts of the 500WT series, the infrared spectra in the ν (CO) (2110−2230 cm^{-1}; Figure 8) and ν (OH) regions (3300−3800 cm^{-1}; Figure 10) recorded after admission of 133Pa of CO at equilibrium at 77K were decomposed. Analysis of the results for ν (CO) region shows a shift to higher wavenumber in the position of the bands characteristic of Brønsted acid sites from 2153 to 2159 cm^{-1} and from 2160 to 2169 cm^{-1} with increasing W surface density. This is concomitant with a shift to lower wavenumbers observed for the bands characteristic of ν (OH) vibrations. These results are consistent with an overall increase of the mean strength of Brønsted acid sites with increasing W surface density.[54] Similar results were obtained for solids of the 120WT series.

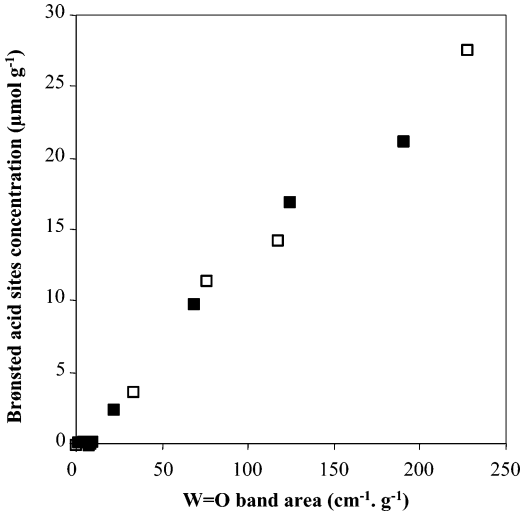

Figure 17. Correlation between ν(W═O) bands area located at 1016 and 1020 cm^{-1} and Brønsted acid sites concentration measured after lutidine desorption at 573 K for 120WT series (□) and 500WT series (■).

4.3.2.3. Assignment of the Bands Attributed to ν(CO) Vibrations. An examination of infrared results relative to low-temperature CO adsorption results indicates a direct relation between the area of the bands at 2150−2160 cm^{-1} in the ν-(CO) region and that of the bands in the ν(OH) region at 3530−3558 cm^{-1} (Figures 13 and 14b). This allows, in accord with the literature,[46,49] the attribution of the bands between 2150 and 2160 cm^{-1} to the interaction of CO molecules with surface hydroxyls (Brønsted acid sites). A band at 2165−70 cm^{-1} has also been detected in the spectra relative to the titania support and the WO_x/TiO_2 catalysts. According to Hadjiivanov and Klissurski,[46] this band is associated with Lewis acid sites of titania, whereas Busca et al.[49] attribute the band to Brønsted acid sites of WO_x/TiO_2 catalysts. In the present study, for solids with a W surface density > 1.6 atoms of W/nm^2, a correlation has been observed between the ν(CO) vibration at 2165−2170 cm^{-1} and the ν(OH) vibration at 3446−3462 cm^{-1}. No such correlation was found for catalysts containing a lower W surface density (Figure 14a). This suggests that the band at 2165−2170 cm^{-1} reflects the presence of Brønsted acid sites for catalysts containing more than 1.6 atoms of W/nm^2 and the presence of a mixture of Lewis and Brønsted acid sites for a lower W surface density.

4.3.2.4. Correlation between the Structure of W Surface Species and Brønsted Acidity. Figure 17 depicts the evolution of the concentration of Brønsted acid sites measured following lutidine desorption at 573 K, as a function of the area of the sum of the two infrared bands at 1016 and 1020 cm^{-1} attributed to the ν(W═O) vibration for the polymerized W species. The results indicate a direct relationship between the abundance of Brønsted acid sites and the area of the bands characteristic of the polymerized W species. This suggests that the latter are associated with the development of Brønsted acid sites.

4.4. Catalytic Activity for 2-Propanol Dehydration: Correlation with Brønsted Acidity. For the 500WT series, an

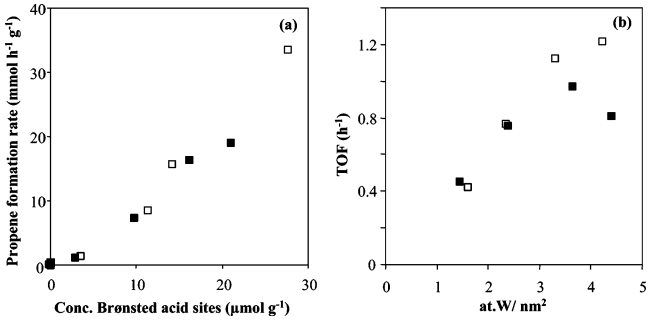

Figure 18. (a) Variation of propene formation rate determined at 403 K and $D = 60$ mL min^{-1} as a function of Brønsted acid sites concentration measured after lutidine desorption at 573 K. (b) "Turnover frequency (TOF)": Propene formation rate (mmol h^{-1} g^{-1}) per Brønsted acid sites measured at 573 K (μmol g^{-1}). 120WT series: (□). 500WT series: (■).

examination of the catalytic activity results for 2-propanol dehydration (Figure 15) shows the presence of a threshold of W loading of 1.3 atoms of W/nm^2 for the development of the activity. Similar behavior has been observed for the same reaction on W supported on titania.[32] In contrast, no indications for the presence of a threshold may be inferred from the results of Sohn and Bae.[33] One may speculate that the apparent disagreement may be attributed to differences in the preparation method leading to the formation of W polymeric species with the initial addition of W.

For the 120WT series, a similar evolution of the catalytic activity with W surface density was observed. Namely, the same minimum of W required for the development of the activity was observed (1.3 atoms of W/nm^2). Furthermore, the results clearly show similar activity for a given W surface density. This suggests that, as observed for the WO_x/ZrO_2 system,[16] the initial form of the support (amorphous titanium oxyhydroxide, 120WT0, or crystalline titania in an anatase form, 500WT0) had little impact on the catalytic activity for 2-propanol dehydration.

Figure 18a shows the variation of propene formation rate as a function of the abundance of Brønsted acid sites measured following the adsorption of lutidine at ambient temperature and desorption at 573 K. Similar results were obtained for the two series. The results indicate an increase in the catalytic activity with an increase in the number of Brønsted acid sites prior to the reaction. One can also note an increase in the slope of the curve with an increase in the abundance of Brønsted acid sites. Assuming a direct relation between the number of Brønsted acid sites prior to the reaction and the number present under reaction conditions, the observed increase in the slope may be taken as an indication of an overall increase in the intrinsic activity per Brønsted acid sites. This is clearly illustrated in Figure 18b, which shows an increase in the turnover frequency (activity per Brønsted acid sites measured at 573 K) with W surface density. Similar behavior was observed for MoO_x/ZrO_2 catalysts[55] and attributed to the development of new Brønsted acid sites.

4.5. Catalytic Activity for *n*-Hexane Isomerization; Correlation with the Structure of W Surface Species. Figure 16 clearly shows that the catalysts of both series (120WT and 500WT) exhibit the same evolution of the catalytic activity for *n*-hexane isomerization. Catalysts containing less than 3.6 atoms of W/nm^2 yielded little or no activity. For a higher W surface density, a sharp increase in activity is observed. The presence of a minimum of W surface density for the development of activity may be inferred from the results reported for pentane isomerization.[54] A comparison of the results of both series shows that the activity is essentially determined by the W surface density and not by the initial form of the support.

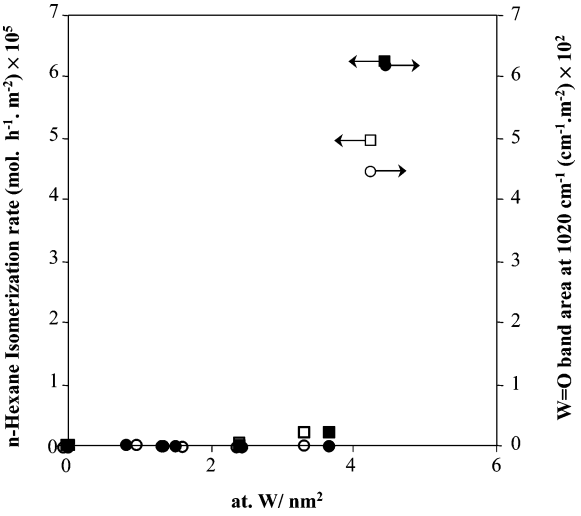

Figure 19. Initial rate of isomerization of *n*-hexane at 523 K and $P(H_2) = 10^3$ KPa (□, ■; left axis) and infrared band area located at 1020 cm^{-1} (○, ●; right axis) versus W surface density. Open symbols: 120WT series. Full symbols: 500WT series.

Figure 19 shows the evolution of the catalytic activity and the area of the band at ca. 1020 cm^{-1}, attributed to the most polymerized W species, with the W surface density. The results suggest that the catalytic activity for *n*-hexane isomerization is associated with the most polymerized W species. The incipient formation of WO_3 observed by Raman spectroscopy for 500W4.4 suggests that these species consist of WO_x multilayers, precursors of WO_3. The sharp increase in isomerization activity for solids with the highest W surface density suggests that these W species, characterized by the IR band at 1020 cm^{-1}, exhibit stronger Brønsted acidity. However, no direct evidence of the presence of these highly acidic sites was found from low-temperature CO adsorption studies. This may be attributed to the low concentration of these acid sites or to the possibility that they are formed under reactions conditions.

4.6. Comparison of the Two Catalytic Tests. For both catalytic tests, a minimum of W surface density appears to be required for the development of catalytic activity. However, a significantly higher threshold for the development of activity is observed for *n*-hexane isomerization (3.6 atoms of W/nm^2 versus 1.3 atoms of W/nm^2 for 2-propanol dehydration). This shift may be attributed to the more demanding character of *n*-hexane isomerization (compared to 2-propanol dehydration). Specifically, stronger Brønsted acid sites associated with larger WO_x domains and characterized by the band at 1020 cm^{-1} may be required.

4.7. Influence of the Initial Form of the Support: Ti Oxyhydroxide or Titanium Oxide in Anatase Form. In their pioneering study, Hino and Arata[13−15] have shown that supported W oxides obtained by the impregnation of hydrated zirconia or titania were active for the reactions of hexane or pentane isomerization, whereas those obtained by deposition of the W phase on a crystalline zirconia or titania were inactive for the same reactions. In contrast, our recent study concerning the WO_x/ZrO_2 system[16] indicated that the initial form of the support (Zr oxyhydroxide or crystallized zirconia) has little impact on the development of the surface structure, acidity, and catalytic property of WO_x/ZrO_2 catalysts. The apparent contradiction with the results of Hino and Arata[15] was attributed to the nature of the crystalline form of the zirconia support (tetragonal versus monoclinic forms). Specifically, it was proposed that the lack of influence observed in our study was due to the close similarities between the surface structure of

amorphous zirconium oxyhydroxide and tetragonal zirconium oxide and that the reported differences in catalytic performances are attributed to the tetragonal/monoclinic composition of the zirconia support. The activity for *n*-hexane isomerization seemed to be associated with the tetragonal form of the support of WO_x/ZrO_2 catalysts.

The results of the present study can, thus, be explained along similar lines. As observed for tungstated zirconia, a detailed analysis of the structure, acidity, and performance of WO_x/TiO_2 catalysts clearly shows no significant influence of the initial form of the support (amorphous Ti oxyhydroxide or titania in the anatase form) on the structure and catalytic properties of WO_x/TiO_2 solids. One may thus speculate that the observed differences in the catalytic properties of WO_x/amorphous Ti oxyhydroxide or crystallized titania reported by Hino and Arata[15] are essentially due to the specific crystalline structure of the titania support (rutile versus anatase in the present study). Indeed, we have verified in a separate experiment[56] that a WO_x/TiO_2 catalyst obtained by impregnation of the rutile support ($S_{BET} = 26.5\ m^2\ g^{-1}$) and containing a W surface density similar to that of active solids was inactive for *n*-hexane isomerization.

5. Conclusions

The influence of W deposition and the crystalline nature of the support (titanium oxyhydroxide versus titania in anatase form) on the surface structure, acidity, and catalytic activity was investigated by XRD, Raman, and infrared spectroscopy and catalytic tests. Two series of WO_x/TiO_2 catalysts containing up to 4.4 atoms of W/nm^2 were prepared by the pore volume impregnation of titanium oxyhydroxide dried at 393 K (120WT series) or titanium oxide calcined at 773 K (500WT series). The following conclusions can be made.

For a given W surface density, the results for the two series clearly showed that catalysts obtained by the impregnation of amorphous titanium oxyhydroxide or titania in the anatase form exhibited similar surface structure, acidity, and catalytic activity. Thus, no significant effect of the initial form of the support (Ti oxyhydroxide versus anatase titanium oxide) on the development of the surface structure and catalytic properties was evidenced.

For both series, Raman and XRD results indicate that W is present essentially as a surface phase. An analysis of the infrared spectra shows a shift to a higher wavenumber in the position of ν(W═O) with increasing W surface density. Brønsted acidity was detected for W > 1.3 atoms of W/nm^2 and increases steadily, in abundance, with increasing W surface density. A correlation between the abundance of Brønsted acid sites and the area of the infrared band at ca. 1016 cm^{-1} attributed to extensively polymerized W species was observed.

A direct relation between the abundance of Brønsted acid sites and catalytic activity for 2-propanol dehydration was evidenced. For the reaction of *n*-hexane isomerization, significant activity was only measured for W surface densities > 3.6 atoms of W/nm^2. The shift to a higher value of the threshold (1.3 atoms of W/nm^2 for 2-propanol dehydration) was ascribed to the more demanding character of the reaction requiring stronger Brønsted acid sites associated with larger WO_x domains.

Acknowledgment. Thanks are due to M. N. Metzner (SIFCOM laboratory, UMR CNRS 6176, ENSICAEN−Université de Caen) for performing the XRD measurements and to M.T. Chatellier and J. Quillard (LCS laboratory, UMR CNRS 6506, ENSICAEN−Université de Caen) for performing the activity measurements.

References and Notes

(1) Gielgens, L. H.; van Kampen, M. G. H.; Broek, M. M.; van Hardeveld, R.; Ponec, V. *J. Catal.* **1995**, *154*, 201.
(2) Benitez, V. M.; Querini, C. A.; Figoli, N. S.; Comelli, R. A. *Appl. Catal., A* **1999**, *178*, 205.
(3) van Schalkwyk, C.; Spamer, A.; Moodley, D. J.; Dube, T. I.; Reynhardt, J.; Botha, J. M. *Appl. Catal., A* **2003**, *225*, 121.
(4) van Schalkwyk, C.; Spamer, A.; Moodley, D. J.; Dube, T. I.; Reynhardt, J.; Botha, J. M.; Vosloo, H. C. M. *Appl. Catal., A* **2003**, *255*, 143.
(5) Spamer, A.; Dube, T. I.; Moodley, D. J.; van Schalkwyk, C.; Botha, J. M. *Appl. Catal., A* **2003**, *255*, 133.
(6) Chen, J. P.; Yang, R. T. *Appl. Catal., A* **1992**, *80*, 135.
(7) Khodayari, R.; Ingemar Odenbrand, C. U. *Ind. Eng. Chem. Res.* **1998**, *37*, 1196.
(8) Lietti, L.; Nova, I.; Ramis, G.; Dall'Acqua, L.; Busca, G.; Giamello, E.; Forzatti, P.; Bregani, C. *J. Catal.* **1999**, *187*, 419.
(9) Orsenigo, C.; Lietti, L.; Tronconi, E.; Forzatti, P.; Bregani, C. *Ind. Eng. Chem. Res.* **1998**, *37*, 2350.
(10) Lietti, L.; Forzatti, P.; Bregani, C. *Ind. Eng. Chem. Res.* **1996**, *35*, 3884.
(11) Alemany, L. J.; Berti, F.; Busca, G.; Ramis, G.; Robba, D.; Toledo, G. P.; Trombetta, M. *Appl. Catal., B* **1996**, *10*, 299.
(12) Herrmann, J. M.; Disdier, J. *Catal. Today* **2000**, *56*, 389.
(13) Arata, K.; Hino, M. Synthesis of Solid Superacid of Tungsten Oxide Supported on Zirconia and Its Catalytic Action. In *Proc. 9th I.C.C.*; Philips, M. J., Ternan, M., Eds.; The Chemical Institute of Canada: Ottawa, Canada, 1988; p 1727.
(14) Hino, M.; Arata, K. *J. Chem. Soc., Chem. Commun.* **1988**, 1259.
(15) Hino, M.; Arata, K. *Bull. Chem. Soc. Jpn.* **1994**, *67*, 1472.
(16) Lebarbier, V.; Clet, G.; Houalla, M. *J. Phys. Chem. B* **2006**, *110*, 13905.
(17) Scholz, A.; Schnyder, B.; Wokaun, A. *J. Mol. Catal. A: Chem.* **1999**, *138*, 249.
(18) Burrows, A.; Devenish, R. W.; Joyner, R. W.; Kiely, C. J.; Knözinger, H.; Lange, F. *Inst. Phys. Conf. Ser.* **1993**, *138* (10), 481.
(19) Vaidyanathan, N.; Houalla, M.; Hercules, D. M. *Catal. Lett.* **1997**, *43*, 209.
(20) Xu, B.; Dong, L.; Fan, Y.; Chen, Y. *J. Catal.* **2000**, *193*, 88.
(21) Wachs, I. E.; Hardcastle, F. D. Raman Spectroscopy of Supported Metal Oxides on Al_2O_3, TiO_2, and SiO_2: A Comparative Study; Philips, M. J., Ternan, M., Eds.; The Chemical Institute of Canada: Ottawa, Canada, 1988; Vol. 3, p 1449.
(22) Yu, X. F.; Wu, N. Z.; Huang, H.-Z.; Xie, Y. C.; Tang, Y. Q. *J. Mater. Chem.* **2001**, *11*, 3337.
(23) Fiedor, J. N.; Houalla, M.; Proctor, A.; Hercules, D. M. *Surf. Interface Anal.* **1995**, *23*, 234.
(24) Eibl, S.; Gates, B. C.; Knözinger, H. *Langmuir* **2001**, *117*, 107.
(25) Bond, G. C.; Flamerz, S.; Van Wijk, L. *Catal. Today* **1987**, *1*, 229.
(26) Kim, D. S.; Ostromecki, M.; Wachs, I. E. *J. Mol. Catal. A: Chem.* **1996**, *106*, 93.
(27) Vermaire, D. C.; van Berge, P. C. *J. Catal.* **1989**, *116*, 309.
(28) Engweiler, J.; Harf, J.; Baiker, A. *J. Catal.* **1996**, *159*, 259.
(29) Ramis, G.; Busca, G.; Cristiani, C.; Lietti, L.; Forzatti, P.; Bregani, F. *Langmuir* **1992**, *8*, 1744.
(30) Papp, J.; Soled, S.; Dwight, K.; Wold, A. *Chem. Mater.* **1994**, *6*, 496.
(31) Ma, Z.; Hua, W.; Tang, Y.; Gao, Z. *J. Mol. Catal. A: Chem.* **2000**, *159*, 335.
(32) Onfroy, T.; Clet, G.; Bukallah, S. B.; Visser, T.; Houalla, M. *Appl. Catal., A* **2006**, *298*, 80.
(33) Sohn, J. R.; Bae, J. H. *Korean J. Chem. Eng.* **2000**, *17*, 86.
(34) Hilbrig, F.; Schmelz, H.; Knözinger, H. Acidity of WO_x/TiO_2 Catalysts for Selective Catalytic Reduction (SCR). In *New Frontiers in Catalysis, Proc. 10th ICC*; Gusczi, L., Solymosi, F., Tétényi, P., Eds.; Elsevier: Amsterdam, 1993; Vol. 75, p 1351.
(35) Yamagushi, T.; Tanaka, Y.; Tanabe, K. *J. Catal.* **1980**, *65*, 442.
(36) Patrono, P.; La Ginestra, A.; Ramis, G.; Busca, G. *Appl. Catal., A* **1994**, *107*, 249.
(37) Onfroy, T.; Clet, G.; Houalla, M. *Microporous Mesoporous Mater.* **2005**, *82*, 99.
(38) Vuurman, M. A.; Wachs, I. E.; Hirt, A. M. *J. Phys. Chem.* **1991**, *95*, 9928.
(39) Gutiérrez-Alejandre, A.; Castillo, P.; Ramirez, J.; Ramis, G.; Busca, G. *Appl. Catal., A* **2001**, *216*, 181.
(40) Lahousse, C.; Maugé, F.; Bachelier, J.; Lavalley, J. C. *J. Chem. Soc., Faraday Trans.* **1995**, *91*, 2907.
(41) Ziolek, M.; Kujawa, J.; Saur, O.; Aboulayt, A.; Lavalley, J. C. *J. Mol. Catal. A: Chem.* **1996**, *112*, 125.
(42) Travert, A.; Manoilova, O. V.; Tsyganenko, A. A.; Mauge, F.; Lavalley, J. C. *J. Phys. Chem. B* **2002**, *106*, 1350.

(43) Lahousse, C.; Aboulayt, A.; Bachelier, J.; Lavalley, J. C. *J. Mol. Catal.* **1993**, *84*, 283.
(44) Hadjiivanov, K.; Lamotte, J.; Lavalley, J. C. *Langmuir* **1997**, *13*, 3374.
(45) Busca, G.; Saussey, H.; Saur, O.; Lavalley, J. C.; Lorenzelli, V. *Appl. Catal.* **1985**, *14*, 245.
(46) Hadjiivanov, K.; Klissurski, D. *Chem. Rev.* **1996**, *25*, 61.
(47) Bolis, V.; Fubini, B.; Garrone, E.; Morterra, C.; Ugliengo, P. *J. Chem. Soc., Faraday Trans.* **1992**, *88*, 391.
(48) Bolis, V.; Fubini, B.; Garrone, E.; Morterra, C. *J. Chem. Soc., Faraday Trans.* **1989**, *85*, 1383.
(49) Busca, G.; Martra, G.; Zecchina, A. *Catal. Today* **2000**, *56*, 361.
(50) Zaki, M. I.; Knözinger, H. *Spectrochim. Acta* **1987**, *43*, 1455.
(51) Hadjiivanov, K.; Vayssilov, G. N. *Adv. Catal.* **2002**, *47*, 307.
(52) Afanasiev, P.; Geantet, C.; Breysse, M.; Coudurier, G.; Vedrine, J. C. *J. Chem. Soc., Faraday Trans.* **1994**, *90*, 193.
(53) Ostromecki, M. M.; Burcham, L. J.; Wachs, I. E.; Ramani, N.; Ekerdt, J. G. *J. Mol. Catal. A: Chem.* **1998**, *132*, 43.
(54) Eibl, S.; Jentoft, R. E.; Gates, B. C.; Knözinger, H. *Phys. Chem. Chem. Phys.* **2000**, *2*, 2565.
(55) Samaranch, B.; Ramirez de la Piscina, P.; Clet, G.; Houalla, M.; Homs, N. *Chem. Mater.* **2006**, *18*, 1581.
(56) Lebarbier, V.; Clet, G.; Houalla, M. Unpublished results.